

The equilibrium constant for reaction 4.40 is:

$$K = \frac{a_{\text{Mg}_3\text{Al}_2\text{Si}_3\text{O}_{12}}}{a_{\text{Mg}_2\text{Si}_2\text{O}_6} a_{\text{MgAl}_2\text{SiO}_6}} \quad (4.41)$$

where the activities in the denominator represent the activities of the enstatite and the hypothetical aluminous enstatite phase components in the enstatite solid solution. In the pure MgO system (i.e., no CaO, FeO, MnO, etc.), the numerator, the activity of pyrope, is 1, of course, and we may write:

$$\begin{aligned} \Delta G^\circ &= RT \ln(a_{\text{Mg}_2\text{Si}_2\text{O}_6} a_{\text{MgAl}_2\text{SiO}_6}) \\ &= \Delta H^\circ - T\Delta S^\circ + (P - P_{\text{ref}})\Delta V^\circ \end{aligned} \quad (4.42)$$

(compare eqn. 4.37). For an ideal case, this may be rewritten as:

$$\begin{aligned} RT \ln(X_{\text{Mg}_2\text{Si}_2\text{O}_6} X_{\text{MgAl}_2\text{SiO}_6}) \\ = \Delta H^\circ - T\Delta S^\circ + (P - P_{\text{ref}})\Delta V^\circ \end{aligned} \quad (4.43)$$

Wood and Banno (1973) first estimated thermodynamic parameters (ΔH , ΔS , and ΔV for aluminous pyroxene) from experimental data. They dealt with the non-ideality in two ways. First, they assumed ideal solution behavior at 1 bar and assumed all non-ideality associated with substitution of Al in orthopyroxene at higher pressure could be accounted for in the volume term in eqn. 4.42, which they rewrote as:

$$\Delta \bar{V} = \bar{V}_{\text{Mg}_3\text{Al}_2\text{Si}_3\text{O}_{12}}^\circ - \bar{V}_{\text{Mg}_2\text{Si}_2\text{O}_6}^{\text{opx}} - \bar{V}_{\text{MgAl}_2\text{SiO}_6}^{\text{opx}} \quad (4.44)$$

As for non-ideality related to substitution of Ca and Fe in the system, they noted that non-idealities of most silicate systems were of similar size and magnitude and hence the activity coefficients for garnet tend to cancel those for orthopyroxene. Furthermore, the ΔV and ΔH terms are both large and tend to reduce the errors due to non-ideal behavior.

Complexities arise because Fe, Ca, and Cr are also present in both garnet and orthopyroxene at significant concentrations. In addition, the available thermodynamic data (based on experiments) has greatly improved and, consequently, a number of studies have improved on and extended the work of Wood and Banno. Brey and Köhler (1990) developed equations that took advantage of the

new data and took account of Cr and Ca concentrations; these were further refined by Brey *et al.* (2008). Some of the simplifying assumptions originally made by Wood and Banno, such as ideal mixing between Mg and Fe in garnet and pyroxene and between Mg and Al in orthopyroxene, were retained, but other aspects required more complex, asymmetric solution models to match experimental data. Simplifying things somewhat by assuming a Cr-, Na-, and Ti-free system, their expression for pressure is:

$$P(\text{GPa}) = \frac{-C_2 \sqrt{C_2^2 + 0.004 C_3 C_1}}{20 C_3} \quad (4.45)$$

where

$$\begin{aligned} C_1 &= -RT \ln K + 4970 + 84.15T - 19T^{1.2} \\ &\quad + 3(X_{\text{Ca}}^{\text{Grt}})^2 \times 82456 \\ &\quad + X_{\text{Mg}}^{\text{M1}} X_{\text{Fe}}^{\text{M1}} (80941 - 36.3T) \\ &\quad - 3X_{\text{Mg}}^{\text{Grt}} X_{\text{Fe}}^{\text{Grt}} \times 17795 \\ C_2 &= -0.533 - 1.62 \times 10^{-4}(T - 298) \\ &\quad + 3(X_{\text{Ca}}^{\text{Grt}})^2 \times 3.305 \\ C_3 &= -7.2 \times 10^{-4} \end{aligned}$$

and

$$K = \frac{(1 - X_{\text{Ca}}^{\text{Grt}})^3}{X_{\text{MF}}^{\text{M1}} X_{\text{MF}}^{\text{M2}} X_{\text{MF}}^{\text{M2}} X_{\text{Al}}^{\text{M1}}} \quad (4.46)$$

The mole fractions $X_{\text{MF}}^{\text{M1}}$ and $X_{\text{MF}}^{\text{M2}}$ are the mole fractions of Mg+Fe in the M1 and M2 sites respectively, i.e.:

$$X_{\text{MF}}^{\text{M2}} = 1 - \text{Ca} - \text{Na} - \text{Ti}$$

and

$$X_{\text{MF}}^{\text{M1}} = \text{Al} / 2$$

Ca, Na, and Ti are assumed to occupy only the M2 octahedral site; Al is assumed to be evenly divided, as required by charge balance, between the M1 octahedral site and the tetrahedral site (otherwise occupied by Si). Since ideal mixing between Mg and Fe is assumed:

$$X_{\text{Mg}}^{\text{M2}} = X_{\text{MF}}^{\text{M1}} \times \text{Mg} / (\text{Mg} + \text{Fe})$$

and

$$X_{\text{Fe}}^{\text{M1}} = X_{\text{MF}}^1 - X_{\text{Mg}}^{\text{M1}}$$

Garnet mole fractions are defined as:

$$X_{\text{Ca}}^{\text{Grt}} = \text{Ca} / (\text{Ca} + \text{Mg} + \text{Fe} + \text{Mn})$$

$$X_{\text{Fe}}^{\text{Grt}} = \text{Fe} / (\text{Ca} + \text{Mg} + \text{Fe} + \text{Mn})$$

The full equations of Brey *et al.* (2008) are slightly more complex because they take account of the effect of Cr in garnet and Na in pyroxene. A spreadsheet for the calculations, PTEXL.xls, is available from the authors at <http://www.mineralogie.uni-frankfurt.de/petrologie-geochemie/mitarbeiter/brey/downloads/index.html>.

Since eqns. 4.42 and 4.45 contain temperature as well as pressure terms, it is obvious that the temperature must be known to calculate pressure of equilibration. In the same paper, Wood and Banno (1973) provided the theoretical basis for estimating temperature from the orthopyroxene–clinopyroxene miscibility gap, which we discuss later. Thus in a system containing garnet, orthopyroxene and clinopyroxene, both temperature and pressure of equilibration may be estimated from the composition of these phases.

This geobarometer–geothermometer is commonly used to estimate the temperature and pressure (depth) of equilibration of mantle-derived garnet lherzolite xenoliths. One of the first applications was by Boyd (1973), who calculated P and T for a number of xenoliths in South African kimberlites, and hence reconstructed the geotherm in the mantle under South Africa.

4.5.2.2 Solvus equilibria

Solvus equilibria provide a second kind of thermobarometer. Generally, these make better geothermometers than geobarometers. A good example is the ortho- and clinopyroxene system, illustrated in Figure 4.16. The two-pyroxene solvus has been the subject of particularly intensive experimental and theoretical work because ortho- and clinopyroxene coexist over a wide range of conditions in Mg,Fe-rich rocks of the crust and upper mantle.

One of the inherent thermodynamic difficulties with this type of geothermometer is

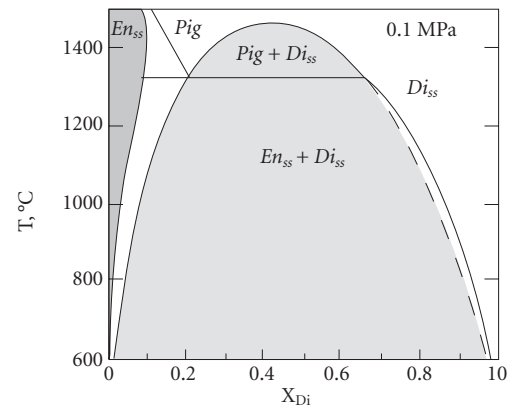


Figure 4.16 Phase relationships in the $\text{Mg}_2\text{Si}_2\text{O}_6$ (enstatite)– $\text{CaMgSi}_2\text{O}_6$ (diopside) system (after Lindsley, 1983). Reproduced with permission.

that since it involves exsolution, ideal solution models will clearly be very poor approximations. Thus considerable efforts have been made to develop solution models for the pyroxenes. Several factors further complicate efforts to use the pyroxene solvus as a thermobarometer. The first is the existence of a third phase, pigeonite (a low-Ca clinopyroxene), at high temperatures and low pressures; the second is that the system is not strictly binary: natural pyroxenes in igneous rocks are solutions of Mg, Ca, and Fe components. The presence of iron is problematic because of the experimental difficulties encountered with Fe-containing systems. These difficulties include the tendency both for iron to dissolve in the walls of commonly-used platinum containers, and for Fe^{2+} either to oxidize to Fe^{3+} or to reduce to metallic iron, depending on the oxygen fugacity. In addition, other components, particularly Na, Ti, and Al, are often present in the pyroxenes.

Despite its complexities, the system has been modeled with some success using a symmetric solution model developed by Wood (1987). Ignoring pigeonite and components other than Ca, Mg and Fe, we can treat mixing in the M2 and M1 sites separately. Mixing in the M2 site can be treated as a ternary Mg, Fe, and Ca solution. In a symmetric ternary solution consisting of components A, B, and C, the activities of the components may be calculated from:

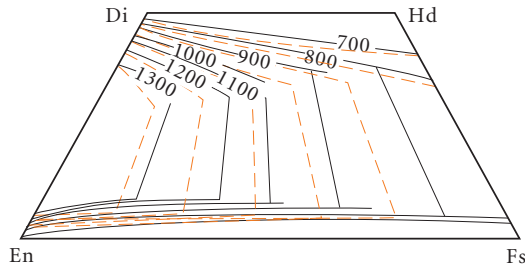
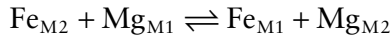


Figure 4.17 Comparison of calculated (solid lines) and experimentally observed (red dashed lines) phase relationships between clino- and orthopyroxene shown in the “pyroxene quadrilateral”, a part of the CaSiO_3 – MgSiO_3 – FeSiO_3 system. Di, diopside; En, enstatite; Hd, hedenbergite; Fs, ferrosilite. Lines show the limit of solid solution at the corresponding temperatures ($^{\circ}\text{C}$). Data from Lindsley (1983).

$$RT \ln \gamma_A = X_B^2 W_G^{AB} + X_C^2 W_G^{AC} + X_B X_C (W_G^{AB} + W_G^{AC} - W_G^{BC}) \quad (4.47)$$

where W_G^{AB} is the A–B binary interaction parameter, and so on. Mixing of Fe and Mg between the M1 and M2 sites was treated as a simple exchange reaction:



with ΔH of 29.27 kJ/mol and ΔS of 12.61 J/mol. Using this approach, Wood calculated the temperature dependence of the solvus as shown in Figure 4.17. The model fits experimental observation reasonably well for the Mg-rich pyroxenes, but significant deviations occur for the Fe-rich pyroxenes.

The complexities of this system are sufficient that a full and accurate theoretical treatment has not been developed. The most widely used implementation of the two-pyroxene geothermometer is an empirical one of Brey and Köhler (1990) where temperature is given by:

$$T = \frac{23664 + (249 + aX_{\text{Fe}}^{\text{cpx}})P}{13.38 + (\ln K_D)^2 + bX_{\text{Fe}}^{\text{opx}}} \quad (4.48)$$

where

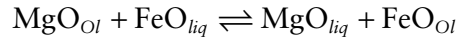
$$K_D = \frac{1 - Ca^{\text{cpx}} / (1 - Na^{\text{cpx}})}{1 - Ca^{\text{opx}} / (1 - Na^{\text{opx}})} \quad (4.49)$$

and $a = 1263$, $b = 11.59$, $X_{\text{Fe}} = \text{Fe}/(\text{Fe} + \text{Mg})$, and P is in GPa. Since solving for P using eqn. 4.47 requires knowing T and solving eqn. 4.48 for T requires knowing P , solving for both requires an iterative approach: making an initial guess of P and T , solving the equations, and repeating the procedure with new values until two successive answers agree within error, which is roughly $\pm 15\text{K}$ and $\pm 0.3\text{GPa}$.

4.5.2.3 Exchange reactions

Exchange reaction thermobarometers depend upon the exchange of two species between phases. We will consider two examples of these.

The Roeder and Emslie (1970) olivine-liquid geothermometer is a rather simple one based on the equilibrium between magma and olivine crystallizing from it. Consider the exchange reaction:



where *Ol* denotes olivine and *liq* denotes liquid. We can write the equilibrium constant for this reaction as:

$$K_D = \frac{X_{\text{FeO}}^{\text{Ol}} X_{\text{MgO}}^{\text{liq}}}{X_{\text{FeO}}^{\text{liq}} X_{\text{MgO}}^{\text{Ol}}} \quad (4.50)$$

Recalling our criteria for a good geothermometer, we can guess that this reaction will meet at least several of these criteria. First, olivine exhibits complete solid solution, so we might guess we can treat it as an ideal solution, which turns out to be a reasonably good assumption. We might also guess that the molar volumes of forsterite and fayalite and of their melts will be similar, meaning the ΔV term, and hence pressure dependence, will be small, which is also true. As it turns out, however, the ΔH term, which is related to the difference in heats of fusion of forsterite and fayalite, is also relatively small, so the exchange reaction itself is a poor geothermometer. However, we can consider two separate reactions here:



and we can write two expressions for K_D . This was the approach of Roeder and Emslie (1970), who deduced the following relations from empirical (i.e., experimental) results:

$$\log \frac{X_{\text{MgO}}^{\text{Ol}}}{X_{\text{MgO}}^{\text{liq}}} = \frac{3740}{T} - 1.87 \quad (4.51)$$

and

$$\log \frac{X_{\text{FeO}}^{\text{Ol}}}{X_{\text{FeO}}^{\text{liq}}} = \frac{3911}{T} - 2.50 \quad (4.52)$$

These K_D s are much more temperature-dependent than for the combined exchange reaction. Subtracting eqn. 4.51 from 4.52 yields:

$$\log K_D = \frac{171}{T} - 0.63 \quad (4.53)$$

where K_D is defined as in eqn. 4.50. Note that these equations have the form of eqn. 3.95. Roeder and Emslie (1970) used these equations to construct the diagram in Figure 4.18.

Subsequent work has shown that K_D as defined in equation has a weak dependence on pressure and the silica activity of the melt. Toplis (2005) describes a method to account for these effects. Example 4.3

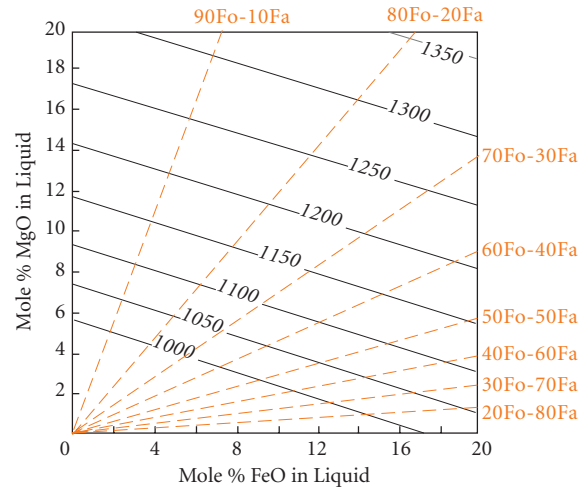


Figure 4.18 Olivine saturation surface constructed by Roeder and Emslie (1970). With kind permission of Springer Science+Business Media.

Example 4.3 Calculating magma temperatures using the olivine geothermometer

From the electron microscope analysis of a mid-ocean ridge basalt glass and its coexisting olivine microphenocrysts, calculate the temperature at which the olivine and liquid equilibrated.

Answer: We will answer this assuming the glass composition represents that of the liquid and using eqns. 4.51 and 4.52. We first have to convert the analysis of the glass from weight percent to mole fraction.

SiO ₂	50.3
Al ₂ O ₃	14.3
ΣFeO	11.1
MgO	7.8
CaO	11.5
Na ₂ O	2.6
K ₂ O	0.23
MnO	0.20
TiO ₂	1.71
Total	99.02
Mol % Fo in Ol	82

Let's set up a spreadsheet to do these calculations. First we deal with the Fe analysis. The analysis reports only iron as FeO. Generally, about 10% of the iron in a basalt will be present as ferric iron (Fe₂O₃), so we will have to assign 10% of the total iron to Fe₂O₃. To do this, we get the weight percent FeO simply by multiplying the total FeO by 0.9. To get weight percent Fe₂O₃, we multiply total FeO (11.1%) by 0.1, then multiply by the ratio of the molecular weight of Fe₂O₃ to FeO and divide by 2 (since there are 2 Fe atoms per "molecule").

Now we calculate the mole fractions. We'll set up a column with molecular weights and divide each weight percent by the molecular weight to get the number of moles per 100 grams. To convert to mole fraction, we divide the number of moles by the sum of the number of moles.

	wt%	w/10% ferric	Mol. wt	moles	mol frac.
SiO ₂	50.3	50.3	60.09	0.8371	0.5265
Al ₂ O ₃	14.3	14.3	102	0.1402	0.0882
total FeO	11.1	11.1			
FeO		9.99	71.85	0.1390	0.0875
Fe ₂ O ₃		1.22	157.7	0.0077	0.0049
MgO	7.8	7.8	40.6	0.1921	0.1208
CaO	11.5	11.5	56.08	0.2051	0.1290
Na ₂ O	2.6	2.6	61.98	0.0419	0.0264
K ₂ O	0.23	0.23	94.2	0.0024	0.0015
MnO	0.2	0.2	70.94	0.0028	0.0018
TiO ₂	1.71	1.71	79.9	0.0214	0.0135
Total	99.74	99.85		1.590	1.000
XMgO-Ol					0.82
XFeO-Ol					0.18
TMgO		1384	kelvin	1111	°C
TFeO		1390	kelvin	1117	°C

Since the mole fraction of Mg in olivine is equal to the mole fraction of forsterite, we need only convert percent to fraction (i.e., divide by 100). The mole fraction of FeO in olivine is simply $1 - X_{\text{MgO}}$. Thus $X_{\text{MgO(ol)}} = 0.82$ and $X_{\text{FeO(ol)}} = 0.18$. Now we are ready to calculate temperatures. We can calculate two temperatures: one from MgO and the other from FeO. The temperature based on the FeO exchange is:

$$T_{\text{FeO}} = \frac{3911}{\log\left(\frac{X_{\text{FeO}}^{\text{Ol}}}{X_{\text{FeO}}^{\text{liq}}}\right) + 2.50}$$

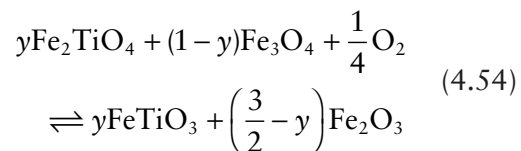
and that based on MgO is:

$$T_{\text{MgO}} = \frac{3740}{\log\left(\frac{X_{\text{MgO}}^{\text{Ol}}}{X_{\text{MgO}}^{\text{liq}}}\right) + 1.87}$$

illustrates the use of the Roeder and Emslie geothermometer.

The iron-titanium oxide system evaluated by Buddington and Lindsley (1964) was one of the first means of obtaining quantitative estimates of crystallization temperatures of igneous rocks. It is important not only because it is useful over a wide range of temperatures and rock types, but also because it yields oxygen fugacity as well. Figure 4.19 shows

the TiO₂-FeO-Fe₂O₃ (rutile-wüstite-hematite) ternary system. The geothermometer is based on the reaction:



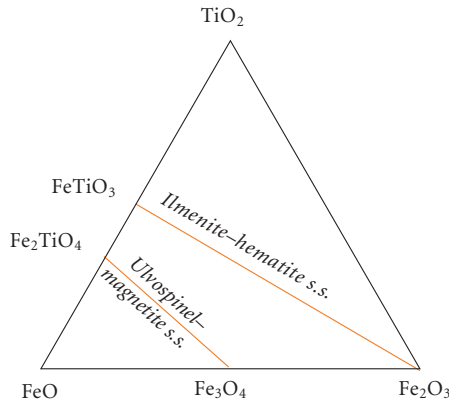
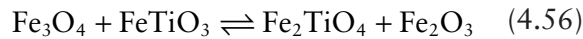


Figure 4.19 The TiO_2 - FeO - Fe_2O_3 ternary system. Phases are: FeO , wüstite; Fe_2O_3 , hematite; TiO_2 , rutile; Fe_2TiO_4 , ulvospinel; Fe_3O_4 , magnetite; FeTiO_3 , ilmenite. The system also includes the FeTi_2O_5 - Fe_2TiO_5 solution, which is not shown.

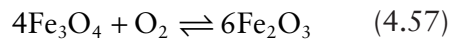
which describes equilibrium between the ulvospinel-magnetite (titanomagnetite) and ilmenite-hematite solid solution series. The equilibrium constant expression may be written as:

$$K = \frac{a_{\text{FeTiO}_3}^y a_{\text{Fe}_2\text{O}_3}^{3/2-y}}{a_{\text{Fe}_2\text{TiO}_4}^y a_{\text{Fe}_3\text{O}_4}^{1-y} f_{\text{O}_2}^{1/4}} \quad (4.55)$$

The original Buddington and Lindsley geothermometer was based on empirical observations of compositional dependence on oxygen fugacity and temperature, as shown in Figure 4.20. Having values for the compositions of the titanomagnetite and ilmenite phases, one simply read T and f_{O_2} from the graph. To understand the system from a thermodynamic perspective, it is better to consider the two fundamental reactions occurring separately in this system:



magnetite + ilmenite \rightleftharpoons ulvospinel + hematite
and:



The first reaction represents a temperature-dependent exchange between the titanomagnetite and ulvospinel solutions; the second

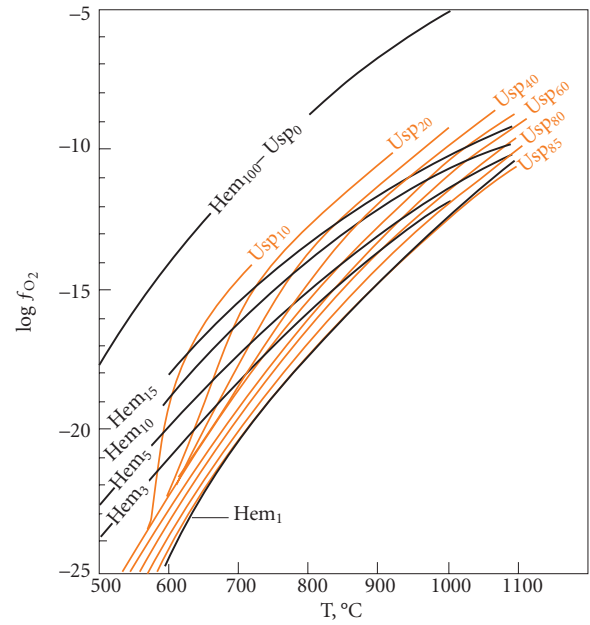


Figure 4.20 Relationship of composition of coexisting titanomagnetite and ilmenite to temperature and oxygen fugacity. Spencer and Lindsley (1981). Reproduced with permission.

reaction is the oxidation of magnetite to hematite.

Several investigators have studied the iron-titanium oxides attempting to improve upon the work of Buddington and Lindsley (1964). The approach of Spencer and Lindsley (1981) was to consider two reactions 4.56 and 4.57. They modeled the ilmenite as a binary asymmetric Margules solution and titanomagnetite as a binary asymmetric Margules solution below 800°C and as an ideal binary solution above 800°C. They modeled configurational entropy-based ordering of Fe^{2+} , Fe^{3+} , and Ti^{4+} in the ilmenite lattice structure (they assumed Fe^{3+} mixed randomly with Ti^{4+} in A sites and Fe^{3+} and Fe^{2+} randomly in B sites). The ΔG of reactions above were written as:

$$-\frac{\Delta G^\circ}{RT} = \ln \left[\frac{X_{\text{Usp}}^\alpha (1 - X_{\text{Ilm}})^\alpha}{(1 - X_{\text{Usp}})^\alpha X_{\text{Ilm}}^\alpha} \right] + \ln \left[\frac{\lambda_{\text{Usp}}^\alpha \lambda_{\text{Hem}}^\alpha}{\lambda_{\text{Mt}}^\alpha \lambda_{\text{Ilm}}^\alpha} \right] \quad (4.58)$$

and:

$$-\frac{\Delta G}{RT} = \ln \left[\frac{X_{\text{Hem}}^{6\alpha}}{X_{\text{M}}^{4\alpha}} \right] + \ln \left[\frac{\lambda_{\text{Hem}}^{6\alpha}}{\lambda_{\text{Mt}}^{6\alpha}} \right] - \ln f_{\text{O}_2} \quad (4.59)$$

Table 4.1 Margules parameters for ilmenite and titanomagnetite solid solutions.

	Usp (<800°C)	Mag (<800°C)	Ilm	Hem
W_H (joules)	64835	20798	102374	36818
W_S (joules)	60.296	19.652	71.095	7.7714
W_G (>800°C) (joules)	0	0		
ΔS_{Usp}^o (joules)	4.192			
ΔH_{Usp}^o (joules)	27799			

From Spencer and Lindsley (1981). Reproduced with permission of the Mineralogical Society of America.

The α parameter is related to the number of sites involved in the exchange; Spencer and Lindsley assumed α was 2 for ilmenite and 1 for titanomagnetite. The excess free energy was expressed in the usual way for an asymmetric solution (eqn. 4.16):

$$\bar{G}_{ex} = (W_{G1}X_2 + W_{G2}X_1)X_1X_2$$

for each solution series. When the effect of pressure is neglected, the free energy interaction parameter expression (eqn. 4.8) simplifies to:

$$W_G = W_H - TW_S \quad (4.60)$$

Values for W_H and W_S were obtained from least-squares fits to experimental data. The parameters obtained are listed in Table 4.1.

Substituting eqns. 4.60 and 4.16 into the free energy of solution expression ($\Delta G_{excess} = \Delta G_{ideal} - \Delta G_{real}$), the following equation can be obtained:

$$T(K) = \frac{AW_H^{Usp} - BW_H^{Mt} - CW_H^{Il} + DW_H^{Hem} + \Delta H^o}{AW_S^{Usp} - BW_S^{Mt} - CW_S^{Il} + DW_S^{Hem} + \Delta S^o - R \ln K^{exch}} \quad (4.61)$$

Oxygen fugacity is determined as:

$$\log f_{O_2} = \log MH$$

$$+ \frac{1}{RT} \left[\frac{12 \ln(1 - X_{ilm}) - 4 \ln(1 - X_{Usp}) + \left[\begin{array}{l} 8X_{Usp}^2(X_{Usp} - 1)W_G^{Usp} + \\ 4X_{Usp}^2(1 - 2X_{Usp})W_G^{Mt} + \\ 12X_{ilm}^2(1 - X_{ilm})W_G^{Ilm} - \\ 6X_{ilm}^2(1 - 2X_{ilm})W_G^{Hem} \end{array} \right]}{2.303} \right] \quad (4.62)$$

where:

$$A = 3X_{Usp}^2 - 4X_{Usp} + 1, B = 3X_{Usp}^2 - 2X_{Usp},$$

$$C = 3X_{ilm}^2 - 4X_{ilm} + 1, D = 3X_{ilm}^2 - 2X_{ilm}$$

$$K^{exch} = \frac{(X_{Usp}X_{Hem}^2)}{(X_{Mt}X_{ilm}^2)}, \quad \Delta H^o = 27.799 \text{ kJ/mol},$$

$$\Delta S^o = 4.1920 \text{ J/K-mol}$$

and MH is the magnetite-hematite buffer (see Example 4.4): $\log MH = 13.966 - 24634/T$.

A number of subsequent studies have further refined the iron–titanium oxide geothermometer based on new experimental data and more sophisticated thermodynamic models. The most recent of these efforts is that of Ghiorso and Evans (2008), whose formulation is too complex to describe here. Software for computing temperature and oxygen fugacity based on their formulation is available at www.ofm-research.org/publications.html.

We have reviewed just a few of the available thermobarometers in use. These were selected to illustrate the underlying principles. There are, however, many thermobarometers in use by geochemists and petrologists. Some of these are listed in Table 4.2.

4.6 THERMODYNAMIC MODELS OF MAGMAS

Silicate liquids have played an extremely important role in the development of the Earth, as well as other bodies in the solar system. As we shall see, the Earth's crust formed as melts from the mantle rose to

Example 4.4 Using the iron–titanium oxide geothermometer

An electron microprobe analysis of oxide phases in an andesite reveals that there is 68 mole percent of ulvospinel in an ulvospinel–magnetite phase, and 93.3% of ilmenite in an ilmenite–hematite phase. Calculate the temperature and f_{O_2} at which these phases equilibrated.

Answer: We can use eqns. 4.61 and 4.62 to answer this question. The data in Table 4.1 are relevant to the binary asymmetric solution model for the system below 800°C. Above 800°C, an ideal solution is assumed for the ulvospinel–magnetite phase, so the interaction parameters for this phase go to 0. But if we don't know the temperature, how do we know which equation to use? We begin by computing temperature using the parameters for less than 800°C. If the temperature computed in this way is greater than 800°C (1073 K), we set the W_H and W_S for ulvospinel and magnetite to 0 and recompute.

XUsp	XIlm		
0.68	0.933		
ΔH	27799		
ΔS	4.192		
R	8.314		
Interaction	Parameters		
WHU	64835	WSU	60.296
WHM	20798	WSM	19.652
WHI	102374	WSI	71.095
WHH	36818	WSH	7.7714
A	−0.3328		
B	0.0272		
C	−0.12053		
D	0.745467		
K	0.010958		
$T = \frac{(A \cdot WHU - B \cdot WHM - C \cdot WHI + D \cdot WHH + \Delta H)}{(A \cdot WHU - B \cdot WHM - C \cdot WSI + D \cdot WSH + \Delta S - R \cdot \ln(K))}$			
T (<800)	1281 K	1008°C	
T (>800)	1205 K	932°C	
$W_G = W_H - T \cdot W_S$			
WGU	−7829.52	WGI	16695.29
WGM	−2885.21	WGH	27452.45
		MH	−6.47
		Log f_{O_2} (<800)	−12.58
		Log f_{O_2} (>800)	−12.69

Once we have temperature, we can compute the W_G terms using the relationship $W_G = W_H - TW_S$, bearing in mind that $W_{Gusp} = W_{GMt} = 0$ if the temperature is greater than 800°C. With these values in hand, we can use eqn. 4.62 to calculate the f_{O_2} . Our spreadsheet is shown here.

These data were taken from one of Spencer and Lindsley's (1981) experiments, performed at 938°C and $\log f_{O_2} = -12.76$. Our calculations are in good agreement with the experimental observation.

the surface and cooled. Thus an understanding of igneous processes is an essential part of earth science. Until a few decades ago, the primary approaches to igneous petrology were observational and experimental. Results

of melting experiments in the laboratory were used to interpret observations of igneous rocks. This approach proved highly successful and is responsible for most of our understanding of igneous processes. However, such

Table 4.2 Commonly used thermobarometers.

Reaction	Type	Reference
Al in hornblende $2\text{SiO}_2 + 2\text{CaAl}_2\text{Si}_2\text{O}_8 + \text{K}(\text{Mg,Fe})_3\text{AlSi}_3\text{O}_{10}(\text{OH})_2 = \text{Ca}(\text{Fe,Mg})_3\text{Al}_4\text{Si}_6\text{O}_{22}(\text{OH})_2$	Displaced equilibria	Anderson and Smith (1995)
Amphibole–plagioclase $\text{NaCa}_2\text{Mg}_5\text{AlSi}_7\text{O}_{22}(\text{OH})_2 + 4\text{SiO}_2 \rightleftharpoons \text{Ca}_2\text{Mg}_5\text{Si}_8\text{O}_{22}(\text{OH})_2 + \text{NaAlSi}_3\text{O}_8$ $\text{NaCa}_2\text{Mg}_5\text{AlSi}_7\text{O}_{22}(\text{OH})_2 + \text{NaAlSi}_3\text{O}_8 \rightleftharpoons \text{Na}(\text{NaCa})\text{Mg}_5\text{Si}_8\text{O}_{22}(\text{OH})_2 + \text{CaAl}_2\text{Si}_2\text{O}_8$	Displaced equilibria	Holland and Blundy (1994)
Calcite = dolomite $\text{CaCO}_3 \rightleftharpoons (\text{Ca,Mg})\text{CO}_3$	Solvus equilibria	Goldsmith and Newton (1969)
Calcite = aragonite $\text{CaCO}_3 \rightleftharpoons \text{CaCO}_3$	Univariant	Johannes and Puhan (1971)
Garnet = biotite Fe-Mg $(\text{Fe,Mg})_3\text{Al}_2\text{Si}_3\text{O}_{12} \rightleftharpoons \text{K}(\text{Mg,Fe})\text{AlSi}_3\text{O}_{10}(\text{OH})_2$	Exchange	Ferry and Spear (1978)
Garnet + quartz = plagioclase + wollastonite $(\text{Fe,Ca})_3\text{Al}_2\text{Si}_3\text{O}_{12} + \text{SiO}_2 \rightleftharpoons (\text{Ca,Na})\text{Al}_2\text{Si}_2\text{O}_8 + 2\text{CaSiO}_3$	Displaced equilibria	Gasparik (1984b)
Hercynite + quartz = garnet + sillimanite $\text{FeAl}_2\text{O}_4 + 5\text{SiO}_2 \rightleftharpoons \text{Fe}_3\text{Al}_2\text{Si}_3\text{O}_{12} + \text{Al}_2\text{SiO}_5$	Displaced equilibria	Bohlen <i>et al.</i> (1986)
Ilmenite + Al_2SiO_5 = garnet + rutile + quartz $3\text{FeTiO}_3 + \text{Al}_2\text{SiO}_5 \rightleftharpoons 3\text{TiO}_2 + (\text{Fe,Ca})_3\text{Al}_2\text{Si}_3\text{O}_{12} + \text{SiO}_2$	Displaced equilibria	Bohlen <i>et al.</i> (1983)
Plagioclase–liquid $\text{CaAl}_2\text{Si}_2\text{O}_8 + \text{NaO}_{0.5}^{\text{liq}} + 2\text{SiO}_2^{\text{liq}} = \text{NaAlSi}_3\text{O}_8 + \text{CaO}^{\text{liq}} + 2\text{AlO}_{1.5}^{\text{liq}}$	Exchange	Kudo and Weill (1970), Putirka (2005)
Plagioclase = garnet + kyanite + quartz $3(\text{Ca,Na})\text{Al}_2\text{Si}_2\text{O}_8 \rightleftharpoons (\text{Fe,Ca})_3\text{Al}_2\text{Si}_3\text{O}_{12} + 2\text{Al}_2\text{SiO}_5 + \text{SiO}_2$	Displaced equilibria	Ghent (1976), Koziol and Newton (1988)
Ti in zircon–Zr in rutile $\text{ZrSiO}_4 + \text{TiO}_2 \rightleftharpoons \text{ZrTiO}_4$ $\text{ZrSiO}_4 + \text{TiO}_2 \rightleftharpoons \text{ZrO}_2(\text{in rutile}) + \text{SiO}_2$	Exchange	Ferry and Watson (2007)

an approach has inherent limitations: virtually every magma is unique in its composition and crystallization history. Yet the experimental database is limited: it is not practical to subject every igneous rock to melting experiments in the laboratory. Realizing this, igneous petrologists and geochemists turned to thermodynamic models of silicate melts as a tool to interpret their evolution. With a proper “model” of the interaction of various components in silicate melts and adequate thermodynamic data, it should be possible to predict the equilibrium state of any magma under any given set of conditions. The obstacles in developing proper thermodynamic models of silicate liquids, however, have been formidable. Because they are stable only at high temperatures, obtaining basic thermodynamic data on silicate liquids is difficult. Furthermore, silicate liquids are very complex solutions, with eight or more elements present in high enough concentrations to affect the properties of the solution. Nevertheless, sufficient progress has been made on these problems that thermody-

namics is now an important tool of igneous petrology.

4.6.1 Structure of silicate melts

As was the case for silicate solids and electrolyte solutions, application of thermodynamics to silicate liquids requires some understanding of the interactions that occur on the atomic level. Thus we will once again have to consider the microscopic viewpoint before developing a useful thermodynamic approach. In this section, we briefly consider the nature of silicate melts on the atomic level.

Most, though not all, of our knowledge of the structure has come from studies of glasses rather than melts. While the thermodynamic properties of silicate liquids and their respective glasses differ, other studies have confirmed the general structural similarities of glasses and liquids. Spectral studies of glasses, which in some respects can be viewed as supercooled liquids, have revealed that silicate liquids have structures rather similar to

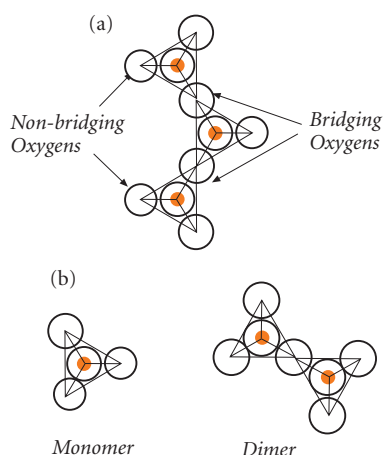


Figure 4.21 Silicate structures. (a) Short-range silicate structures in melts resemble those in solids. Individual tetrahedra may be linked by bridging oxygens and linked to 2 silicon atoms. (b) Units in silicate melts may include monomers, with no bridging oxygens, and dimers, where only 1 of 4 oxygens in each tetrahedra are “bridging”.

those of silicate solids. In fact, the principal difference between silicate liquids and solids is the absence of long-range ordering in the former; short-range ordering is similar. As in silicate minerals, the primary structural element of silicate liquids is the silicon tetrahedron (see Figure 1.11), consisting of a silicon atom surrounded by four oxygens. As in silicate minerals, tetrahedra may be linked by a shared oxygen, called a *bridging oxygen*; not surprisingly, unshared oxygens are termed *non-bridging* (Figure 4.21a). Unlinked silica tetrahedra, that is, those with no bridging oxygens, are termed *monomers*, SiO_4^{4-} (Figure 4.21b). Two tetrahedra linked by a single oxygen are termed *dimers* and have the formula $\text{Si}_2\text{O}_7^{6-}$. Tetrahedra may also be linked by two oxygens to form infinite chains; these have a chemical formula of SiO_3^{2-} . In silicates such as quartz and feldspar, the tetrahedra are all linked into a framework, and all oxygens are shared. All these structural elements can be present in silicate glasses.

The degree to which the silica tetrahedra are linked, or *polymerized*, in silicate liquids affects chemical and physical properties. The degree of polymerization in turn depends on other cations present. These may be divided

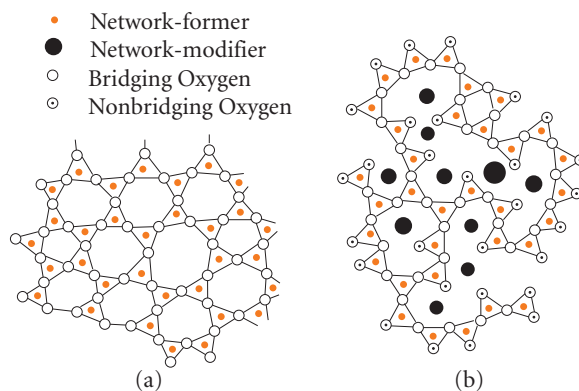


Figure 4.22 (a) Structure of pure silica glass and (b) a silica-rich glass with additional component ions.

into two groups, *network formers* and *network modifiers*. Relatively small, highly charged cations such Al^{3+} and Fe^{3+} (more rarely, Ti^{4+} , P^{3+} , and B^{3+} also) often substitute for silicon in tetrahedral sites and, along with Si, are termed *network formers*. The other common cations of natural silicate liquids, Ca^{2+} , Mg^{2+} , K^+ , Na^+ , and H^+ , are network modifiers. These ions cannot substitute for silicon in tetrahedra and their positive charges can only be balanced by non-bridging oxygens. Addition of these ions disrupts the linkages between silica tetrahedra. Thus as silicate melts become richer in these network modifiers they become progressively depolymerized. This is illustrated in Figure 4.22, which compares the structure of pure silica glass (liquid) and a silica-rich glass (liquid). Melt structure in turn affects the physiochemical properties of the melt. For example, SiO_2 -rich melts tend to have low densities and high viscosities. As ions such as MgO or CaO are added to the melt, viscosity decreases and density increases as the polymer structure is disrupted.

4.6.2 Magma solution models

Advances on several fronts have moved thermodynamic modeling of magmas from an academic curiosity to a useful petrological tool. First, spectroscopic (mainly Raman and infrared spectroscopy, both of which are sensitive to atomic and molecular vibrations) studies are revealing the structure of silicate

melts, which provides the theoretical basis for thermodynamic models. Second, more sophisticated thermodynamic models more accurately reflect interactions in silicate melts. Third, the thermodynamic database has become more complete and more accurate. Finally, the wide accessibility and power of computers and appropriate programs have made the extensive matrix calculations involved in these models possible.

Several factors complicate the task of thermodynamic modeling of magmas. First, magmas are solutions of many components (typically eight or more). Second, the solids crystallizing from magmas are themselves solutions. Third, magmas crystallize over a substantial temperature range (as much as 400–500°C, and more in exceptional cases). Furthermore, crystallization may occur over a range of pressures as a magma ascends through the Earth, and crystallization may be accompanied by melting and assimilation of the surrounding country rock. Despite these complications, several models that are sufficiently accurate to be useful to petrologists have been published, most notably those of Ghiorso (Ghiorso *et al.*, 1983; Ghiorso and Sack, 1995) and Nielsen and Dungan (1983). The goal of these models is to describe the phases and their proportions in equilibrium with a magma, and the resulting evolution of liquid composition. In particular the models of Ghiorso and colleagues are applicable to both melting and crystallization. In section 4.6.2.1, we briefly consider the model of Ghiorso.

4.6.2.1 The regular solution model of Ghiorso and others: “MELTS”

Ghiorso and colleagues (Ghiorso *et al.*, 1983, 2002; Ghiorso, 1987; Ghiorso and Sack, 1995) noted that silicate liquids have substantial compositional regions in which immiscibility occurs and therefore argued that the simplest model that might be able to describe them is the regular solution model. As we saw earlier in the chapter, regular solution models attempt to describe excess functions with interaction, or Margules, parameters. The

Margules equation for excess Gibbs free energy for many components is:

$$\bar{G}_{ex} = \frac{1}{2} \sum_i \sum_{j, j \neq i} X_i X_j W_G^{i,j} \quad (4.63)^*$$

and the Gibbs free energy is:

$$\begin{aligned} \bar{G} = & \sum_i X_i \mu_i^o + RT \sum_i X_i \ln X_i \\ & + \frac{1}{2} \sum_i \sum_j X_i X_j W_G^{i,j} \end{aligned} \quad (4.64)^\dagger$$

The chemical potentials of individual components are:

$$\begin{aligned} \mu_i = \mu_i^o = & +RT \ln X_i + \sum_{j, j \neq i} X_j W_G^{i,j} \\ & - \frac{1}{2} \sum_{j, j \neq k, k \neq j} X_j X_k W_G^{j,k} \end{aligned} \quad (4.65)$$

and the activity coefficients are:

$$RT \ln \lambda_i = \sum_j X_j W_G^{i,j} - \frac{1}{2} \sum_j \sum_k X_j X_k W_G^{j,k} \quad (4.66)$$

Having chosen a general form for the solution model, the next step is to select the components. For practical reasons, Ghiorso *et al.* (1983) placed all components on an 8-oxygen basis. Ghiorso and Sack (1995) chose liquid components that were “mineral-like”: SiO₂, TiO₂, Al₂O₃, Fe₂O₃, MgCr₂O₄, Fe₂SiO₄, Mg₂SiO₄, CaSiO₃, KAlSiO₄, and so on, and H₂O. For components of solid phases, they chose pure end-member *phase* components (e.g., MgSiO₃ in orthopyroxene). The problem with this approach is that the concentrations of these components varied greatly; for example, the mole fraction of SiO₂ is typically 0.4 in basaltic magmas whereas that of Mg₂SiO₄ is typically less than 0.1 and that of KAlSiO₄ is typically less than 0.05. We can see from eqn. 4.60 that when X_i is small, the contribution of the interaction parameters for this component, $W_G^{i,j}$, to the free energy will also be small. Consequently, in the most

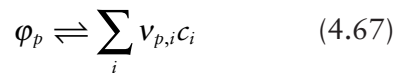
* The $\frac{1}{2}$ term arises because the sum contains both $X_i X_j W_G^{i,j}$ and $X_j X_i W_G^{j,i}$ terms and $W_G^{ij} = W_G^{ji}$.

† For clarity, we have simplified Ghiorso’s equation by neglecting H₂O, which they treated separately.

recent version of this model, called p_{MELTS} , Ghiorso *et al.* (2002) redefined the liquid components so that their mole fractions were more similar, e.g., $\text{SiO}_2 \rightarrow \text{Si}_4\text{O}_8$, $\text{Na}_2\text{SiO}_3 \rightarrow \text{NaSi}_{0.5}\text{O}_{1.5}$.

The next task is to find values for the interaction parameters. These can be calculated from solid–liquid equilibria experiments. The principle involved is an extension of that which we used in constructing phase diagrams: when a solid and liquid are in equilibrium, the chemical potential of each component in each phase must be equal. Since thermodynamic properties of the solids involved are available (determined using standard thermodynamics techniques), the thermodynamic properties of the coexisting liquid may be calculated.

The reaction of a solid phase, ϕ , with the melt can be described with a set of p reactions of the form:



where ϕ_p is the p th end-member component of phase ϕ , c_i refers to the formula for the i th component in the liquid, and $v_{p,i}$ refers to the stoichiometric coefficient of this component. Thus for reaction of olivine with the liquid, we have two versions of eqn. 4.63:



and



We can express the Gibbs free energy change for each of these reaction as:

$$\Delta\bar{G}_r = \Delta\bar{G}_{\phi_p}^o + RT \sum_i v_{p,i} \ln a_i^\ell - RT \ln a_{\phi_p} \quad (4.69)$$

where a_i^ℓ is the activity of the oxide component in the liquid and ϕ_p refers to phase component p in phase ϕ . $\Delta\bar{G}_r$ is, of course, 0 at equilibrium. For example, for reaction 4.63a, we have:

$$\Delta\bar{G}_r = 0 = \Delta\bar{G}_{Fo}^o + RT [2 \ln a_{\text{MgO}}^\ell + \ln a_{\text{SiO}_2}^\ell] + RT \ln a_{Fo}$$

where the subscript Fo refers to the forsterite (Mg_2SiO_4) component in olivine and the superscript ℓ refers to the liquid phase. Expanding the liquid activity term, we have:

$$0 = \Delta\bar{G}_{\phi_p}^o + RT \sum_i v_{p,i} \ln X_i^\ell + RT \sum_i v_{p,i} \ln \lambda_i^\ell - RT \ln a_{\phi_p} \quad (4.70)$$

Substituting eqn. 4.66 for the activity coefficient term in eqn. 4.69 and rearranging to place the “knowns” on the left-hand side, we have:

$$\begin{aligned} -\Delta\bar{G}_{\phi_p}^o + RT \ln a_{\phi_p} - RT \sum_i v_{p,i} \ln X_i^\ell \\ = \sum_i v_{p,i} \sum_j X_j W_G^{i,j} - \frac{1}{2} \sum_j \sum_{k,k \neq j} X_k X_j W_G^{k,j} \end{aligned} \quad (4.71)$$

The quantities on the left-hand side of the equation are terms that can be calculated from the compositions of coexisting solids and liquids and solution models of the solids. The right-hand side contains the unknowns. One statement of eqn. 4.70 can be written for each component in each solid phase at a given temperature and pressure. With enough experiments, values for the interaction parameters can be extracted from the phase relations. Ghiorso *et al.* (1983) and Ghiorso and Sack (1995) used a statistical technique called least squares* to determine the interaction parameters from a large amount of published experimental data. Ghiorso and Sack (1995) also noted that the absence of a phase in an experiment provides thermodynamic information about that phase, in that its free energy must be higher than that of the phases that are present. Their approach made use of this information as well, though discussion of that aspect of their method would take us too far afield. In all, Ghiorso and Sack (1995) used

* “Least squares” is a numerical technique that attempts to minimize the square of the difference between calculated and observed values of some parameter. The square is taken to give greater weight to large deviations. Thus least squares techniques yield results where there are relatively few large deviations between the calculated and observed value of the parameter of interest. We discuss this technique further in Chapter 8.

Table 4.3 Interaction parameters for the Ghiorso regular solution model.

	SiO ₂	TiO ₂	Al ₂ O ₃	Fe ₂ O ₃	MgCr ₂ O ₄	Fe ₂ SiO ₄	Mg ₂ SiO ₄	CaSiO ₃	Na ₂ SiO ₃	KAlSiO ₄	Ca ₃ (PO ₄) ₂
TiO ₂	26267										
Al ₂ O ₃	-39120	-29450									
Fe ₂ O ₃	8110	-84757	-17089								
MgCr ₂ O ₄	27886	-72303	-31770	21606							
Fe ₂ SiO ₄	23661	5209	-30509	-179065	-82972						
Mg ₂ SiO ₄	3421	-4178	-32880	-71519	46049	-37257					
CaSiO ₃	-864	-35373	-57918	12077	30705	-12971	-31732				
Na ₂ SiO ₃	-99039	-15416	-130785	-149662	113646	-90534	-41877	-13247			
KAlSiO ₄	-33922	-48095	-25859	57556	75709	23649	22323	-17111	6523		
Ca ₃ (PO ₄) ₂	613892	25939	52221	-4214	5342	87410	-23209	37070	15572		
H ₂ O	30967	81879	-16098	31406		28874	35634	20375	-96938	10374	43451

Values are in kJ/mol. From Ghiorso and Sack (1995). With kind permission of Springer Science+Business Media.

data from 1593 published laboratory experiments. The interaction parameters they determined are listed in Table 4.3. In constructing the *pMELTS* model, Ghiorso *et al.* (2002) used mineral–liquid equilibrium constraints derived from published results of 2439 different laboratory experiments.

One of the goals of *pMELTS* was to improve the thermodynamic predictions at higher pressures. Since many melting reactions involve significant volume changes, this required an improved equation of state for the liquid, that is, an improved description of the relationship between volume and pressure. Ghiorso *et al.* (2002) chose a third-order Birch-Murnaghan equation:

$$P = \frac{3}{2}K \left[\left(\frac{V^\circ}{V} \right)^{\frac{1}{3}} - \left(\frac{V^\circ}{V} \right)^{\frac{5}{3}} \right] \left\{ 1 - \frac{3}{4}(4 - K') \left[\left(\frac{V^\circ}{V} \right)^{\frac{3}{2}} - 1 \right] \right\} \quad (4.72)$$

where K is the bulk modulus. New experimental data on density derived from new shock wave experiments and new experimental determinations of silicate liquid density (by suspending olivine crystals in the liquid and observing if they sink or float) were used to constraint the K' parameter. A new equa-

tion of state for water was also incorporated into *pMELTS*.

With values for the interaction parameters, the model can then be used to predict the assemblage of solids, their compositions, and the liquid composition that will be present in the system as a function of temperature and pressure. The equilibrium condition for a magma, as for any other system, is the condition where Gibbs free energy is at a minimum. Thus the problem becomes finding compositions for the liquid and coexisting solids that minimize G at a particular temperature and pressure. In other words, we want to find values of G_ℓ and $G_{\phi 1}, G_{\phi 2}, \dots, G_{\phi n}$ such that G_{sys} is minimal where:

$$G_{\text{sys}} = G_\ell + \sum_{\phi} G_{\phi} \quad (4.73)$$

Inherent in the problem is finding which solids will be in equilibrium with the liquid for a given bulk system composition at specified temperature and pressure. In Ghiorso's approach, an initial guess is made of the state of the system. This is done by taking the liquid composition as equal to the system composition and estimating what phases are likely to be in equilibrium with this liquid. Then G is expanded as a three-term Taylor Series* about that initial point, N' , where N' is the

* A Taylor series expansion of a function $f(z)$ in the vicinity of some point $z = a$ has the form:

$$f(z) = f(a) + \frac{(z-a)}{1!} f'(a) + \frac{(z-a)^2}{2!} f''(a) + \dots$$

where f' and f'' are the first and second derivatives of f with respect to z .

composite vector containing the mole fractions describing the compositions of all phases in the system. The second term in the expansion is the matrix of first derivatives of G with respect to n_i , the moles of component i , which is simply the matrix of the chemical potentials. A minimum of G occurs where the first derivative is 0. Thus the second term is set to 0 and solution sought by successive iterations. After each iteration, N' is reset to the composition found in the most recent iteration. This approach clearly involves repetitive matrix calculations and would not be practical without a computer, but they can easily be performed on the current generation of computers.

The goal of a thermodynamic model such as MELTS is to predict both the composition of the melt and composition of coexisting solid phases if temperature, pressure and the composition of the system can be specified. Thus such a program should be able to predict the composition of the melt generated in a region undergoing melting and how the composition of that melt evolves as it rises and cools nearer the surface. Figure 4.23 compares the predictions of the 1995 and 2002 versions of the model with experimentally determined compositions of the liquid pro-

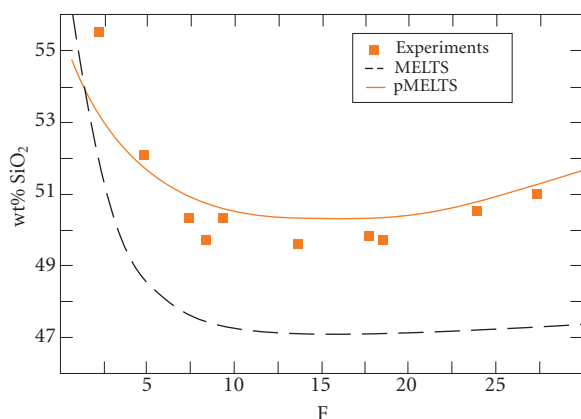


Figure 4.23 SiO_2 concentrations in a melt produced by melting of peridotite at 1 GPa as a function of F , the percent fraction of melt in the system. Figure compares the predictions of the earlier version of the MELTS model, the newer version, $p\text{MELTS}$, and experimentally determined composition. After Ghiorso *et al.* (2002). Reproduced with permission of the American Geophysical Union.

duced by melting peridotite at 1 GPa. The agreement between the model and experimental observation is clearly improved in $p\text{MELTS}$, but it is also clear that the predictions still do not agree perfectly with observations.

Figure 4.24 compares the compositions of clinopyroxene crystals found in basaltic lavas of Cameroon Line volcanoes with the compositions predicted by $p\text{MELTS}$ to crystallize from these magmas. Diamonds and circles are *megacrysts*, and are likely to have crystallized from the magmas. Stars are pyroxenes in ultramafic xenoliths, which are more likely pieces of mantle accidentally incorporated into the magma. The kink in the lower link reflects the onset of garnet crystallization. The agreement is not perfect but this diagram nevertheless shows the enormous value of this thermodynamic approach in igneous petrology. In this example, Rankenburg *et al.* (2004) were able to estimate the pressure and temperature of crystallization as 1400°C and 1.7–2.3 GPa. These pressures correspond to depths greater than the thickness of the crust in this area, hence the authors concluded the pyroxene megacrysts must have crystallized in the mantle. Future refinements of MELTS will undoubtedly close the gap between predictions and observations and enhance the value of this tool.

The latest version of the model, $p\text{MELTS}$ runs on UNIX-based computers (including

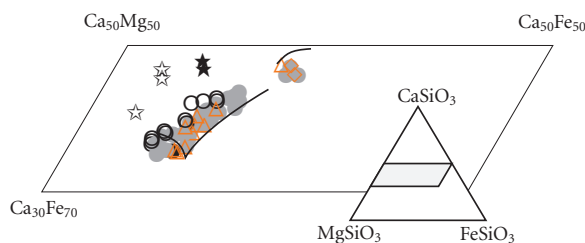


Figure 4.24 Compositions of pyroxenes found in lavas from the Cameroon Line. Diamonds, circles, and triangles are *megacrysts* and likely to have crystallized from these lavas. Stars are pyroxenes in *xenoliths* accidentally incorporated in the lavas. Lines show the compositions of the pyroxenes predicted by $p\text{MELTS}$ to crystallize from these magmas as they cool and evolve. After Rankenburg *et al.* (2004). With kind permission of Springer Science+Business Media.

Mac OS X), and is available on the Internet at <http://melts.ofm-research.org/index.html>. This website also has an online Java version available.

4.7 REPRISE: THERMODYNAMICS OF ELECTROLYTE SOLUTIONS

We discussed the nature of electrolyte solutions and introduced one approach to dealing with their non-ideality, namely the Debye–Hückel activity coefficients, in Section 3.7. We also noted a number of theoretical weaknesses in the Debye–Hückel approach and that this approach is restricted to fairly dilute solutions (ionic strengths less than 0.1 M). In this section we will return to the problem of electrolyte solutions and examine the causes of non-ideal behavior in high ionic strength solutions in more detail. Before doing so, however, we need to introduce a new variation on our now-familiar thermodynamic parameters, namely mean ionic quantities.

4.7.1 Mean ionic quantities

Consider an aqueous NaCl solution. In Chapter 3 we saw that the thermodynamic properties of a salt are related to those of its component ions by:

$$\Psi_{AB} \equiv \nu_A \Psi_A + \nu_B \Psi_B \quad (3.73)$$

So, for example, the chemical potential of NaCl in solution is:

$$\mu_{\text{NaCl}} = \mu_{\text{Na}^+} + \mu_{\text{Cl}^-}$$

which we can express as:

$$\mu_{\text{NaCl}} = \mu_{\text{Na}^+}^o + \mu_{\text{Cl}^-}^o + RT(\ln a_{\text{Na}^+} + \ln a_{\text{Cl}^-}) \quad (4.74)$$

or:

$$\mu_{\text{NaCl}} = \mu_{\text{Na}^+}^o + \mu_{\text{Cl}^-}^o + RT(\ln m_{\text{Na}^+} + \ln m_{\text{Cl}^-}) + RT(\ln \gamma_{\text{Na}^+} + \ln \gamma_{\text{Cl}^-})$$

Though we can certainly determine the concentrations of Na and Cl in solution, how do

we independently determine their activity coefficients? Since we cannot create a pure Na^+ solution or a pure Cl^- one, we cannot say what part of the non-ideality of NaCl solution is due to Na^+ and what part is due to Cl^- . The practical solution then is to assign all non-ideality equally to both ions. This leads to the concept of the *mean ion activity coefficient*:

$$\gamma_{\pm} = (\gamma_{\text{Na}^+} \gamma_{\text{Cl}^-})^{1/2} \quad (4.75)$$

Thus the mean activity coefficient of a salt is the geometric mean of the activity coefficients of its component ions. Equation 4.74 then becomes:

$$\mu_{\text{NaCl}} = \mu_{\text{Na}^+}^o + \mu_{\text{Cl}^-}^o + RT(\ln m_{\text{Na}^+} + \ln m_{\text{Cl}^-} + \ln \gamma_{\pm}^2)$$

Equation 4.75 is valid for 1:1 salts (i.e., 1 cation for each anion). A general expression for the mean activity coefficient of a salt of composition $\text{A}_{\nu^+}\text{B}_{\nu^-}$ is:

$$\gamma_{\pm} = (\gamma_{+}^{\nu^+} \gamma_{-}^{\nu^-})^{1/\nu} \quad (4.76)$$

where ν is the sum of the component positive and negative ions:

$$\nu = \nu^+ + \nu^- \quad (4.77)$$

Mean activity coefficients have the advantage that they are readily measurable (through electrochemical means or solubility, for example). Given a well-behaved salt, such as KCl, where the relationship $\gamma_{-} = \gamma_{+}$ appears to hold, it is then possible to determine single ion activity coefficients. For example, we can obtain γ_{Na^+} in our NaCl solution by first determining γ_{Cl^-} in KCl:*

$$\gamma_{\text{Cl}^-} = \gamma_{\text{K}^+} = \gamma_{\pm\text{KCl}}$$

then determining the mean ion activity coefficient of NaCl experimentally *in a solution of the same ionic strength* and calculating γ_{Na^+} as:

$$\gamma_{\text{Na}^+} = \frac{\gamma_{\pm\text{NaCl}}^2}{\gamma_{\text{Cl}^-}}$$

This is illustrated in Example 4.5.

*The use of KCl as a reference for determining mean ion activity coefficients is based on the observation that K^+ and Cl^- have about the same effective radius and ion mobility; this is known as the MacInnes Convention. Like that of Debye–Hückel, however, this approach breaks down at high ionic strength.

Example 4.5 Calculating single ion activity coefficients from mean ionic activity coefficients

The measured mean ionic activity coefficient of KCl in a solution of 1.0 m ionic strength is 0.604; that of CaCl₂ in a solution of the same ionic strength is 0.449. What is the activity coefficient of Ca²⁺? Assume $\gamma_{\text{Cl}^-} = \gamma_{\text{K}^+}$.

Answer: We begin by noting that $\gamma_{\text{Cl}^-} = \gamma_{\text{K}^+} = \gamma_{\pm\text{KCl}}$ and therefore that $\gamma_{\text{Cl}^-} = 0.604$. According to eqn. 4.76, the mean ion activity coefficient for CaCl₂ is related to the single ion activity coefficients as:

$$\gamma_{\pm\text{CaCl}_2} = (\gamma_{\text{Ca}^{2+}} \gamma_{\text{Cl}^-}^2)^{1/3}$$

Solving this for $\gamma_{\text{Ca}^{2+}}$ we have:

$$\gamma_{\text{Ca}^{2+}} = \frac{\gamma_{\pm\text{CaCl}_2}^3}{\gamma_{\text{Cl}^-}^2} = \frac{0.449^3}{0.604^2} = 0.248$$

We can extend the concept of mean ionic quantities to other thermodynamic variables as well. The *mean ionic potential*, μ_{\pm} , is defined as:

$$\mu_{\pm} = \frac{v_+ \mu_+ + v_- \mu_-}{v} \quad (4.78)$$

Thus the mean ionic potential is simply the arithmetic mean of the potential of the individual ions weighted by their stoichiometric coefficients. We could also express the mean ionic potential as:

$$\mu_{\pm} = \mu_{\pm}^{\circ} + \frac{RT(\ln a_+^{v_+} + \ln a_-^{v_-})}{v} \quad (4.79)$$

Rearranging once more, we obtain:

$$\mu_{\pm} = \mu_{\pm}^{\circ} + RT \ln (a_+^{v_+} a_-^{v_-})^{1/v} \quad (4.80)$$

Comparing this relationship with eqn 4.76, we define a *mean ionic activity* such that:

$$a_{\pm} = (a_+^{v_+} a_-^{v_-})^{1/v} \quad (4.81)$$

We can also define mean ionic molalities such that $a_{\pm} = \gamma_{\pm} m_{\pm}$. Substituting $a_{\pm} = \gamma_{\pm} m_{\pm}$, and $a_+ = \gamma_+ m_+$, we find the *mean ionic molality* is then:

$$m_{\pm} = (m_+^{v_+} m_-^{v_-})^{1/v} \quad (4.82)$$

Mass balance requires that:

$$m_+ = v_+ m \quad \text{and} \quad m_- = v_- m \quad (4.83)$$

Substituting this into eqn. 4.78, we see that:

$$m_{\pm} = m (v_+^{v_+} v_-^{v_-})^{1/v} \quad (4.84)$$

Let's return to our NaCl example. Dissociation is essentially complete and v_+ and v_- are unity, so that:

$$m_{\text{Na}^+} = m_{\text{NaCl}} \quad \text{and} \quad m_{\text{Cl}^-} = m_{\text{NaCl}}$$

Since $v = 2$:

$$m_{\pm\text{NaCl}} = \sqrt{m_{\text{NaCl}}^2} = m_{\text{NaCl}}$$

Mean ionic molality is simply equal to molality for a completely dissociated salt consisting of monovalent ions such as NaCl.

The mean ionic activity coefficient, or the *stoichiometric activity coefficient* as it is sometimes referred to, of NaCl would be the square root of the product of the component activity coefficients according to eqn. 4.82, as would the mean ionic activity. The individual ion activities can be measured in a number of ways. Therefore, the above relationships allow calculation of the mean ionic activity

Example 4.6 Mean ionic parameters for a fully dissociated electrolyte

If the molality of a CaCl_2 solution is 0.3 M and the activity coefficients of Ca^{2+} and Cl^- are 0.5 and 0.7 respectively, calculate the activity and mean ionic molality of CaCl_2 in the solution. Assume that CaCl_2 fully dissociates.

Answer: For CaCl_2 , $v^+ = 1$, $v^- = 2$, and $v = 3$. So we can use eqn 4.84 to calculate mean ionic molality:

$$m_{\pm\text{CaCl}_2} = m_{\text{CaCl}_2} (1^1 2^2)^{1/3} = 4^{1/4} m_{\text{CaCl}_2}$$

Substituting 0.3 for m , we find that $m_{\pm} = 0.4762 \text{ M}$.

We then use eqn. 4.76 to calculate the mean ionic activity coefficient:

$$\gamma_{\pm} = (\gamma_+^{v^+} \gamma_-^{v^-})^{1/v} = (0.5^1 0.7^2)^{1/3} = 0.625$$

The mean ionic activity is then:

$$a_{\pm} = \gamma_{\pm} m_{\pm} = 0.625 \times 0.4762 = 0.298$$

and the activity of CaCl_2 is:

$$a_{\text{CaCl}_2} = a_{\pm}^v = \gamma_{\pm}^v m_{\pm}^v = 0.298^3 = 0.0263 \text{ M}$$

coefficient from measurable quantities (see Example 4.6).

For strong electrolytes, (salts that completely dissociate), it can also be shown that mean activity coefficient and mean activity of the salt are related to its activity coefficient and activity by:

$$\gamma = \gamma_{\pm}^v \quad (4.85)$$

and

$$a = a_{\pm}^v \quad (4.86)$$

We can modify the Debye–Hückel equations to obtain mean ion activity coefficients as follows:

Debye–Hückel Extended Law:

$$\log_{10} \gamma_{\pm} = \frac{-Az_+ |z_-| \sqrt{I}}{1 + B\bar{a} \sqrt{I}} \quad (4.87)$$

Limiting Law:

$$\log_{10} \gamma_{\pm} = -Az_+ |z_-| \sqrt{I} \quad (4.88)$$

where \bar{a} is taken as the sum of the radii of the anion and cation (i.e., $\bar{a} = \bar{a}_+ + \bar{a}_-$).

4.7.1.1 Relationship between activity and molality of a salt

Let's consider the relationship between activity and molality of a salt in an electrolyte solution such as a NaCl solution. Figure 4.25a illustrates this relationship. What we immediately notice is that the slope in the Henry's Law region is essentially zero, which is not at all what we expect for Henry's Law behavior.

It can easily be shown that the relationship in Figure 4.25a is a simple consequence of the dissociation of NaCl into Na^+ and Cl^- ions. From eqn. 3.73 we have:

$$\mu_{\text{NaCl}} = \mu_{\text{Na}^+_{aq}} + \mu_{\text{Cl}^-_{aq}} \quad (4.89)$$

Substituting this into eqn. 3.46, we obtain:

$$\mu_{\text{NaCl}} = \mu_{\text{Na}^+}^o + \mu_{\text{Cl}^-}^o + RT \ln a_{\text{Na}^+} + RT \ln a_{\text{Cl}^-}$$

In the reference state of infinitely dilute solution, $m_i = a_i$, so that:

$$\mu_{\text{NaCl}} = \mu_{\text{Na}^+}^o + \mu_{\text{Cl}^-}^o + RT \ln m_{\text{Na}^+} + RT \ln m_{\text{Cl}^-} \quad (4.90)$$

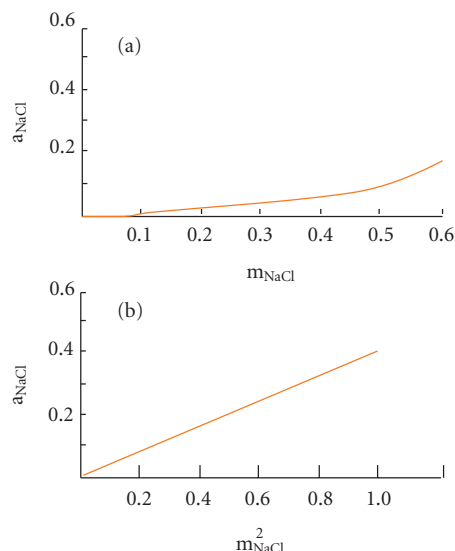


Figure 4.25 (a) Relationship between activity and molality of NaCl in aqueous solution. The activity is very low and the “Henry’s Law Slope” is almost 0 at low concentrations. (b) Relationship between activity and the square of molality of NaCl in aqueous solution.

Furthermore, charge balance requires that:

$$m_{\text{Na}^+} = m_{\text{Cl}^-} = m_{\text{NaCl}} \quad (4.91)$$

Substituting eqn. 4.91 into 4.90 and rearranging:

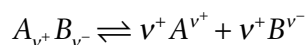
$$\begin{aligned} \mu_{\text{NaCl}} &= \mu_{\text{Na}^+}^o + \mu_{\text{Cl}^-}^o + 2RT \ln m_{\text{NaCl}} \\ &= \mu_{\text{Na}^+}^o + \mu_{\text{Cl}^-}^o + RT \ln m_{\text{NaCl}}^2 \end{aligned} \quad (4.92)$$

Comparing this equation with eqn. 3.46, we see that:

$$a_{\text{NaCl}} \propto m_{\text{NaCl}}^2$$

When we plot activity versus the square of molality, we obtain a linear relationship (Figure 4.25b).

Generalizing this result for dissociation of a substance into a positive ion A and negative ion B, such as:



then the relationship between activity of a salt and its molality is:

$$a_{AB} \propto m_{AB}^{\nu} \quad (4.93)$$

For example, ν is 3 for CaCl_2 , 4 for FeCl_3 , and so on.

Now let’s see what happens if we substitute the mean ion activity for activity. Since:

$$a_{\pm}^{\nu} = a_{AB}$$

$$\text{We have: } a_{\pm}^{\nu} = m_{AB}^{\nu} \quad \text{or} \quad a_{\pm} \propto m_{AB}$$

This is the relationship that we observed in Figure 4.25, so we see that the mean ionic activity accounts for the effects of dissociation.

4.7.2 Activities in high ionic strength solutions

The Debye–Hückel equation becomes inaccurate at ionic strengths above about 0.1 m. This is illustrated in Figure 4.26, which shows the experimentally determined mean ion activity coefficient for NaCl as a function of ionic strength and temperature. At low temperatures, the activity begins to increase ionic strengths of about 1 m, whereas Debye–Hückel predicts continual decrease. The activities of many electrolytes eventually exceed 1 at high concentrations. The difference between the observed activity coefficients and those predicted by the Debye–Hückel equation is due to the effects of ion association and solvation. Debye and Hückel explicitly assumed complete dissociation, i.e., no ion associations, and while their treatment included in a general way the dielectric properties of water, it neglected the effects of solvation. As we noted in Chapter 3, the effects of both ion association and solvation become increasingly important with increasing ionic strength. It should be no surprise then that the Debye–Hückel treatment breaks down at high ionic strength. Here we will consider these effects in greater detail.

4.7.2.1 Correction for the concentration of water

At low and moderate ionic strength, we can assume that the mole fraction of water in solution is 1. For example, in seawater with

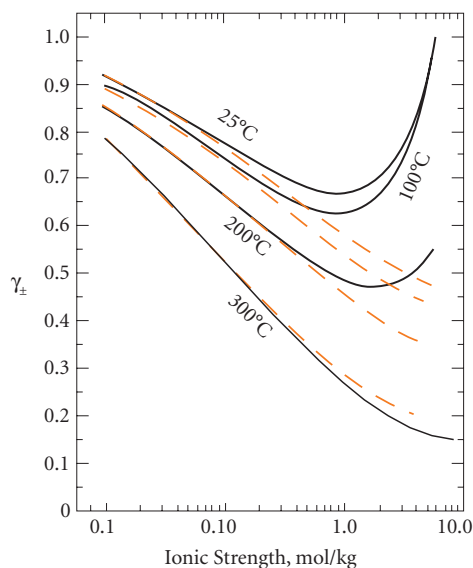


Figure 4.26 Observed mean ion activity coefficient, γ_{\pm} , of NaCl as a function of ionic strength and temperature (solid lines; data from Helgeson *et al.*, 1981) compared with values predicted by the Debye-Hückel Law (dashed red lines, computed as $(\gamma_{\text{Na}^+} \gamma_{\text{Cl}^-})^{1/2}$). After Helgeson *et al.* (1981). Reprinted by permission of the American Journal of Science.

an ionic strength of 0.7, the mole fraction of water about 0.99. Generally, activity coefficients and equilibrium constants are not known within 1%, so the error introduced by this assumption is still small compared with other errors. In higher ionic strengths, however, this assumption is increasingly invalid (for example, at a molality of 3, the mole fraction of water has decreased below 0.95), and this must be taken into account. A convenient way to do this is to incorporate it into the activity coefficient. The corrected activity coefficient is:

$$\gamma_{\text{corr}} = \frac{\gamma}{\left(1 + 0.018 \sum_i m_i\right)} \quad (4.94)$$

4.7.2.2 Effects of solvation

Water molecules bound to ions in solvation shells have lost their independent translational motion and move with the ion as a single entity. These water molecules are effec-

Table 4.4 Ion solvation numbers.

Species	<i>h</i>	Species	<i>h</i>
Li ⁺	2.3	OH ⁻	7.6
Na ⁺	3.3	F ⁻	6.7
K ⁺	2.3	Cl ⁻	2.7
Rb ⁺	2.3	Br ⁻	1.7
Mg ²⁺	8.9	CO ₃ ²⁻	14.4
Ca ²⁺	8.9	SO ₄ ²⁻	10.4
Cd ²⁺	6.3		
Ba ²⁺	9.2		

From Marcus (1985). With permission from John Wiley & Sons.

tively unavailable for reaction, hence solvation has the effect of reducing the activity of water, which increases the apparent concentration, or activity, of the solutes. In addition to solvation (i.e., the direct association of some water molecules with the ion), the charge of the ion causes collapse of the water structure beyond the solvation shell.

For a solution consisting of a single salt, Robinson and Stokes (1959) proposed the contribution of solvation to the mean ion activity coefficient could be expressed as:

$$\log \gamma_{\pm}^{\text{solv}} = -\frac{h}{\nu} \log a_w - \log(1 - 0.018hm) \quad (4.95)$$

where $\gamma_{\pm}^{\text{solv}}$ is the solvation contribution to the mean ion activity coefficient, *h* is the number of moles of water molecules bound to each mole of salt, *a_w* is the activity of water, *m* is the concentration of the salt in solution, and ν is as defined in eqn 4.77 (i.e., total moles of ions produced upon dissolution of a mole of salt). Table 4.4 listed estimated values for the solvation number, that is, the number of water molecules in the solvation shell of each ion. From these, the value of *h* for eqn. 4.95 can be calculated. The activity of water can be adequately estimated as:

$$a_w = 1 - 0.04m$$

Figure 4.27 illustrates the effect of solvation on the activity coefficient. As may be seen, solvation substantially affects the activity coefficient at ionic strengths above about 0.5 m.

4.7.2.3 Effects of ion association

An ion pair can be considered to have formed when ions approach closer than some critical distance, r_c , where the electrostatic energy, which tends to bind them, exceeds twice the thermal energy, which tends to move them apart. When this happens, the ions are electrostatically bound and their motions are linked. They are said to form an ion pair. The thermal energy of an ion is kT and electrostatic interaction energy is:

$$U_{\text{electro}} = \frac{q_1 q_2}{4\pi\epsilon r} \quad (4.96)$$

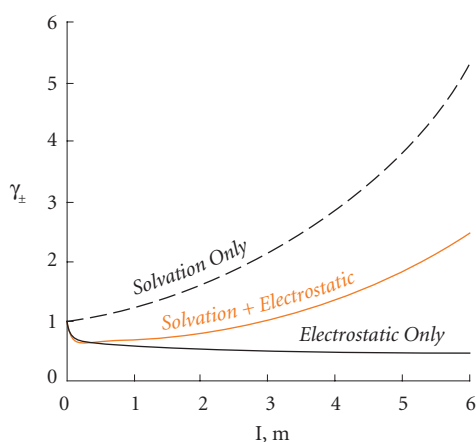


Figure 4.27 Comparison of the electrostatic contribution to the mean ion activity coefficient of NaCl (calculated by the Debye–Hückel Extended Law), the solvation contribution (calculated from eqn. 4.94 assuming $h = 4$) and the sum of the two.

The ratio of these two energies when the distance is less than the critical one is then:

$$\frac{U_{\text{electro}}}{U_{\text{therm}}} = \frac{z_1 z_2 e^2}{4\pi\epsilon_0 \epsilon_r T} \quad (4.97)$$

We can use this equation to solve for the critical distance r_c :

$$r_c = \frac{z_1 z_2 e^2}{4\pi\epsilon_0 \epsilon_r T} \quad (4.98)$$

For two singly charged ions, the critical distance is 3.57 Å. In a 1 molar solution, the average separation between ions is about 12 Å, so even in such a relatively concentrated solution, ion pairs will not form between singly charged ions. Indeed, the critical distance is smaller than the combined Debye–Hückel radii of all pairs of singly charged ions. Thus we do not expect ion associations to form from pairs of singly charged ions under most circumstances. In contrast, the critical distance for ion association between a singly and a doubly charged ion is 70 Å, considerably greater than the sum of their Debye–Hückel radii. It also exceeds the average separation of ions in a 0.01 m solution (about 55 Å), so that even in dilution solutions, we would expect significant ion pair formation for multiply charged ions.

As we saw earlier, all ions in solution are surrounded by a solvation shell of water molecules. This solvation shell may or may not be disrupted when ion pair formation occurs (Figure 4.28). If it is not disrupted, and the two solvation shells remain intact, an *outer*

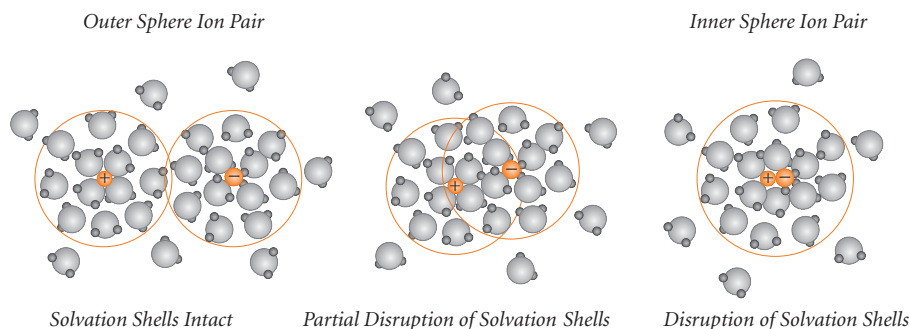


Figure 4.28 In formation of ion pairs, the solvation shells may remain intact or be partially or totally disrupted. The former results in an outer sphere ion pair, the latter results in an inner sphere ion pair.